Multi-MeV Proton Source Investigations in Ultraintense Laser-Foil Interactions

M. Borghesi,[1] A. J. Mackinnon,[2] D. H. Campbell,[3] D. G. Hicks,[2] S. Kar,[1] P. K. Patel,[2] D. Price,[2] L. Romagnani,[1] A. Schiavi,[4] and O. Willi[5]

[1]*Department of Pure and Applied Physics, The Queen's University of Belfast, Belfast BT7 1NN, United Kingdom*
[2]*Lawrence Livermore National Laboratory, Livermore, California 94551, USA*
[3]*The Blackett Laboratory, Imperial College, London SW7 2BZ, United Kingdom*
[4]*Dipartimento di Energetica, Universitá La Sapienza, 00161 Rome, Italy*
[5]*Heinriche-Heine-Universitat, 40225 Dusseldorf, Germany*
(Received 17 February 2003; published 5 February 2004)

A study of the properties of multi-MeV proton emission from thin foils following ultraintense laser irradiation has been carried out. It has been shown that the protons are emitted, in a quasilaminar fashion, from a region of transverse size of the order of 100–200 μm. The imaging properties of the proton source are equivalent to those of a much smaller source located several hundred μm in front of the foil. This finding has been obtained by analyzing proton radiographs of periodically structured test objects, and is corroborated by observations of proton emission from laser-heated thick targets.

The production of protons during ultraintense laser interaction with thin foils is a subject which has recently received a great deal of attention, from both experimental [1–3] and theoretical [4–6] points of view. The protons are accelerated via the space-charge force setup by the displacement of energetic electrons directly accelerated by the laser pulse. The location of the dominant acceleration mechanism is still an object of debate [1–6]. The properties of the proton beam are of interest for a number of important applications, which include the ignition of compressed fusion capsules [7] and probing of laser-plasma experiments [8]. One of the attractions presented by this latter application is the high spatial resolution achievable [8,9] when back-illuminating an object with the proton beam. In a point-projection imaging scheme, this indicates emission from a source with a radius of a few microns. In this Letter we present the results of a series of investigations of the source properties, all consistently showing that protons are emitted in a laminar fashion from an area of the target much larger than suggested by the resolution tests. The imaging properties of this source are equivalent to those of a virtual source located several hundred microns in front of the target. This study is the first to demonstrate directly this very important feature of proton emission, only hinted at in previous work [6]. These results are of primary importance for the correct understanding both of the emission properties of the proton beams and of their envisaged and present applications.

The experiments were carried out using the JanUSP and VULCAN laser facilities, respectively, located at the Lawrence Livermore National Laboratory (LLNL) and at the Rutherford Appleton Laboratory (RAL, U.K.). The chirped pulse amplified (CPA) JanUSP pulse at LLNL has wavelength 0.8 μm and 100 fs duration. It was focused on target by an $f/2$ off-axis parabola (OAP), p polarized, at an angle of incidence of 22°, with a focal spot of 3–5 μm,

full width at half maximum (FWHM). This spot contained 30%–40% of the energy, giving a peak intensity in excess of 10^{20} W/cm^2. The VULCAN laser, operating in the CPA mode, provides 1.054 μm, 1 ps pulses with energy up to 100 J. When focused on target by an F/3.5 OAP (usually p polarized, at a 15° incidence with the target normal), the focal spot varied between 8 and 10 μm in diameter FWHM, containing 30%–40% of the energy (up to 10 J), and giving intensities up to $(5–7) \times 10^{19}$ W/cm^2. The pulses were focused onto the surface of Al foils of various thicknesses, and the protons emitted at the back of the target were detected with stacks of radiochromic film (RCF) and nuclear track detector (CR39) layers. It should be noted here that protons can be accelerated even from a metallic target due to a hydrocarbon (or water vapor) contaminant layer always present at the target surface in standard experimental conditions [10]. The energy spectrum and divergence of the proton beam were consistent with previous observations carried out using the same systems [2,3].

In the JanUSP experiment the proton source (from 3 μm Al foils) was used to backlight static objects. Strong modulations can be imprinted in the proton beam even with thin objects, where the collisional stopping of protons is negligible. The modulations arise from multiple small-angle scattering in the object which increases the local divergence of the beam [11]. In the case of narrow objects, this effect can produce a high-contrast, magnified shadow of the object.

In Fig. 1, shadows of electroformed Cu mesh grids are shown. The meshes are formed by 10 μm lines with 31 μm spacing and 5 μm thickness. The mesh was placed parallel to the proton-producing foil at a distance d from the foil of 0.6 ± 0.05 mm in the case of Fig. 2(a) and 1.0 ± 0.05 mm [Fig. 2(b)]. In both cases the RCF layer shown was located at a distance $L = 23.8 \pm 0.5$ mm from the foil. The position of the layer in the multilayered
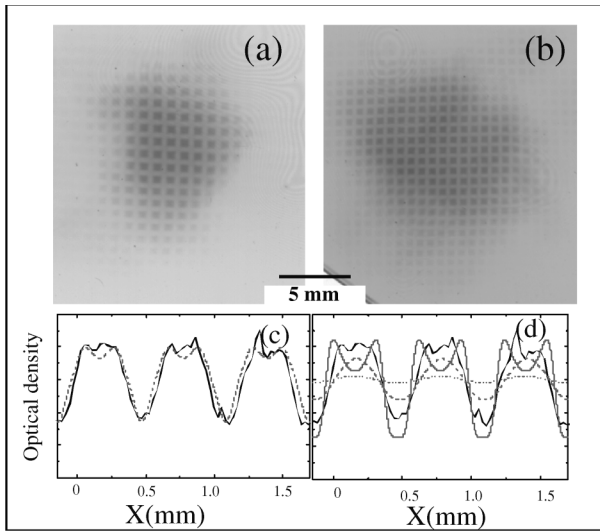
FIG. 1. (a),(b) Shadow of grid meshes (period: 31 μm, linewidth: 10 μm, line thickness: 5 μm) impressed in the proton beam profile, with the grid placed, respectively, at 0.6 and 1 mm from the Al foil producing the protons; the images are collected with RCF placed at 23.8 mm from the Al foil. (c) Profile of optical density (OD, solid line) across mesh shadow in (b). The calculated OD profile for a 10 μm diameter virtual source size is also plotted (dashed line). (d) Comparison between the same experimental OD (solid black line) and calculated profiles for various source sizes (Gaussian sources, $1/e$ beam diameter): 1 μm (gray solid line), 20 μm (dashed line), and 50 μm (dotted line).

detector was such as to record protons with energies around 15 MeV. A line out in optical density (OD) across the shadow of the mesh of Fig. 1(b) is shown in 1(c).

Important information was provided by magnification tests carried out using the periodic structures. The magnification expected for a point-projection imaging scheme is simply the ratio $M_G = L/d$, where L is the source-to-detector distance and d is the source-to-object distance. The experimental magnification was measured in separate shots by placing the mesh at different distances from the target, while the detector was kept at the fixed distance of 23.8 mm. The averaged period of the shadow in the detector plane was divided by the mesh period, yielding the experimental magnification $M_{\exp}$. The measured values of $M_{\exp}$ for various mesh positions are plotted in Fig. 2 against the value of M_G expected, and are consistently smaller than the values expected from purely geometrical considerations. The effect becomes more and more important as the magnification is increased, i.e., as the mesh is placed closer to the source.

This discrepancy can be explained by supposing that the point source is not located at the target plane, but at a distance x in front of the target. In this case the magnification is $M_{\exp} = (L + x)/(d + x) < M_G = L/d$. If one makes this assumption, the experimental magnification $M_{\exp}$ can be expressed as a function of the geometrical magnification M_G expected from a point source located at the target plane, i.e., $M_{\exp} = M_G(L + x)/(L + M_G x)$. The
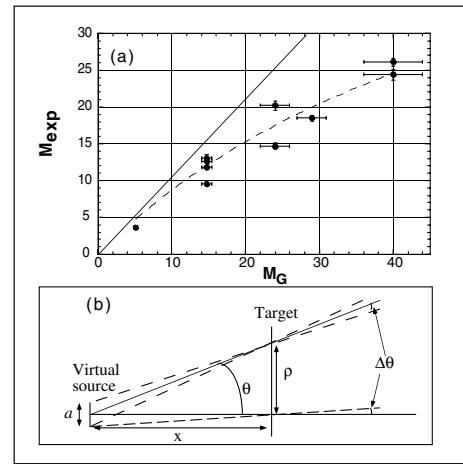
FIG. 2. (a) Plot of experimental magnification versus predicted geometrical magnification for meshes backlit with 15 MeV laser-produced protons; the dashed line is the best fit using the function defined in the text, while the solid line corresponds to $M_{\exp} = M_G$; the error bars for $M_{\exp}$ and M_G arise from experimental uncertainties in the measurement of the distances L and d, and of the periods of the mesh grid and its shadow in the detector. (b) Sketch illustrating the virtual source description of quasilaminar emission from the target.

data of Fig. 2 have been fitted using such a function, where $L = 23.8$ mm and x is a free parameter. As can be seen, the fit reproduces remarkably well the trend of the data. The best fit, plotted in Fig. 3, gives $x \sim 400$ μm. The standard deviation due to shot-to-shot fluctuations is approximately $\Delta x \sim 150$ μm. The average $1/e$ radius of the proton beam at the detector plane is $R = 0.5$ cm (with a shot-to-shot random error of 0.1 cm), giving an average
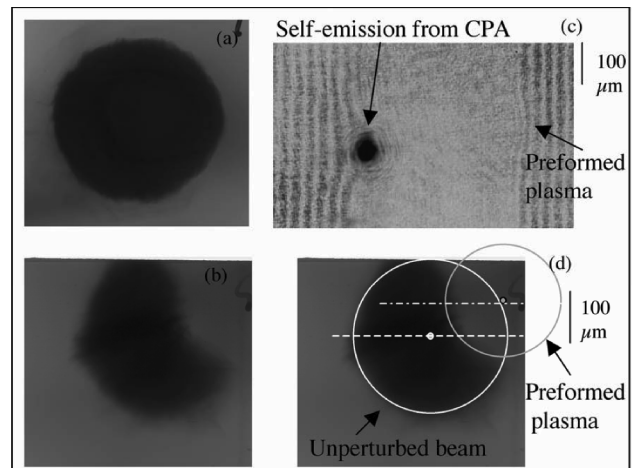
FIG. 3. (a) Proton beam profile on the fourth layer of RCF (corresponding to a beam energy $E \sim 10$ MeV) from an undisturbed Al 250 μm foil. (b) Proton beam profile obtained when a 100 μm radius plasma was preformed on the back of the target. (c) Interferogram showing the preformed plasma at the time of CPA irradiation. (d) Schematic showing the relative position of proton emitting region and preformed plasma on the back surface of the target.

emission half-angle of 11°. The interception of the emission cone at the target plane provides an estimate of the area emitting protons, having a radius ρ of 80 ± 30 μm.

Similar considerations can be inferred by close observation of one of the mesh images. For example, by considering the shadow in Fig. 1(a) one obtains from $M_{\exp} \sim 25$ that the virtual source for the corresponding event was located at $x = 380 \pm 70$ μm in front of the target. The divergence given by the cross section at the detector plane ($R = 4.1 \pm 0.1$ mm) indicates that the beam, if emitted from the virtual source, would encompass an area of the mesh with radius given by $r = R(d + x)/(L + x)$. In our conditions $r = 170 \pm 30$ μm, corresponding to $N = 11 \pm 1$ mesh periods across the proton beam diameter. As a matter of fact, across the experimental cross section one can count ~ 12 and 9 periods, respectively, along a vertical and an horizontal line out, giving an average of 10.5, consistent with the virtual source model. If the point source were located at the target surface, the beam would encompass only 6.5. ± 0.5 mesh periods.

All these considerations are based on the assumption that the protons forming the image are emitted in a quasilaminar fashion, and that, in the absence of collisions, they propagate on a straight line after their emission. This assumption is supported by the fact that the shadow of the mesh is sharp and that the periodicity of the mesh structures does not change across the image. As a matter of fact, if the proton emission were far from laminar, it would not be possible to project an image of the mesh at all. The resolution of a 150 μm nonlaminar source would be equivalent to 5–6 periods of the mesh.

An estimate of the size of the virtual source is provided by a computational code, which has been developed to simulate the proton beam propagation in the conditions of the experiment. The program uses the Monte Carlo calculations provided by the code SRIM [12] to simulate the collisional effects undergone by the protons when traversing matter. The spatially resolved 2D dose distribution and, consequently, the optical density distribution in the RCF layers of the detector are calculated from the SRIM outputs. The experimental parameters for magnification and mesh characteristics are used. The source size can be adjusted until the calculated optical density modulation reproduces the experimental one (details of these calculations will be provided elsewhere). By assuming a Gaussian source, the best match was obtained for a $1/e$ diameter of $a = 10$ μm, which is reproduced in Fig. 1(c). Line outs expected for other source sizes are reproduced in Fig. 1(d), and show the strong dependence of the OD profile from the source size. In Fig. 2(b), "a" is the extension of the virtual source located at a distance x in front of the target, from which the degree of laminarity of the source can be estimated; in other words, a circular section of the proton-emitting region of the target, located at a distance ρ from its center, emits particles within the angle $\theta \pm \Delta\theta$, where $\theta \sim \rho/x$ and $\Delta\theta \sim a/2x \sim 10$ mrad [see Fig. 2(b)]. For such a source, one can roughly

estimate the transverse normalized emittance [13] as $\varepsilon \sim \beta\rho_0\Delta\theta$, where ρ_0 is the radial extent of the proton-emitting area on the back surface of the target and $\beta = v/c$ is the ratio of the proton velocity to the speed of light. By taking the experimental values $\Delta\theta = 10$ mrad and $\rho_0 = 80$ μm, one obtains, for 15 MeV protons, $\varepsilon \sim 0.1\pi$ mm mrad, which compares well with independently reported measurements [14]. Additional effects (e.g., electrostatic charging of the grid) not included in the simple collisional model used could, in principle, lead to even lower estimates for a and ε.

A further study of the proton source characteristics was carried out at the Rutherford Appleton Laboratory using the VULCAN laser. In a previous experiment, it was seen that it was possible to eradicate the proton beam detected at the rear of the target by preforming a plasma at the back of target ahead of the short pulse interaction with the foil [2]. In [2], the heating pulse and the proton-producing pulse focal spots were directly facing each other on opposite sides of the target. Here we present similar results, but obtained with the heating pulse slightly displaced off-axis. The targets used for this test were 250 μm Al foils. A thick foil was chosen in order to decouple front and back surfaces. The CPA Vulcan laser pulse was focused onto the front surface of the foil at an intensity of about 8×10^{19} W/cm^2. The heating pulse (5 J, 600 ps, $\lambda = 0.527$ μm) was focused at an irradiance of 2×10^{13} W/cm^2 onto the rear of the foil, in a focal spot of radius ~ 100 μm. The RCF detector pack was placed at 22 mm from the back of the Al foil. A transverse 4ω probe with ps resolution was employed to obtain interferograms of the preformed plasma. For details of the setup please refer to Fig. 1 of Ref. [2]. In Fig. 3 the proton signal detected onto the fourth RCF layer (corresponding to an energy of 10 MeV) is shown for two different conditions: (a) no heating pulse; (b) heating pulse on, beginning 100 ps before the CPA interaction. The heating pulse was in this case displaced from the axis of the interaction pulse. The amount of vertical displacement can be determined from the corresponding interferogram, taken at the time of CPA irradiation, and shown in Fig. 3(c), by measuring the distance b between the center of symmetry of the preformed plasma and the CPA interaction axis (in this case around 65 μm). The latter can be identified by the self-emission and/or the center of symmetry of the plasma created by CPA on the front of the target. The dimensions of the plasma at the time of the proton production can also be obtained from the interferogram; the density contour corresponding to $n_e = 10^{18}$ cm^{-3} has a radius of approximately 100 μm at the target surface.

While the beam displayed in 3(a) shows the characteristic round shape *always* observed in proton beams produced from thick targets, the shape of the beam cross section is changed in 3(b), as a part of the proton beam appears to be destroyed by the presence of the plasma. The right top corner of the beam has disappeared, and the

cut is with good approximation circular. As shown in Fig. 3(d) a circle with radius ~ 100 μm and with its center at a distance of 65 μm from the CPA interaction axis matches reasonably well the circular cut. The phenomenon was repeatable and the position of the cut changed consistently when the plasma was formed at a different distance from the CPA axis. When the delay was increased by 100 ps, the whole proton beam disappeared, down to the energy cutoff determined by our diagnostic setup ($E \sim 2$ MeV), as observed in [2]. Interferograms indicate that at this time the plasma had a radius ($ne = 10^{18}$ cm^{-3}) of ~ 300 μm.

These observations confirm that the protons and/or the main acceleration mechanism are located at the back surface of the target, and provide a further indication that the protons are emitted from a rather large area. If one takes the distance b as a scale in the target plane, the radius of the area emitting the protons is given as 130 μm. While a plasma with transverse extension of 100 μm is able to inhibit plasma acceleration for only a portion of the beam, a plasma of radius ~ 300 μm is able to cover the whole emitting area and inhibit completely the acceleration process. Two effects can be responsible for this: (1) heating and vaporization of the hydrocarbon layer at the back surface ahead of the arrival of hot electrons from the front, and (2) dramatic decrease of the efficiency of back-surface acceleration due to the increased ion scale length [2]. Also at RAL the virtual source was much smaller than the emitting area. Knife-edge measurements of the proton emittance for similar energies carried out on the same facility indicated a virtual source size of no more than 10 μm.

All these measurements are consistent with quasi-laminar emission from an extended area of the target. Similar conclusions have been obtained, with a different technique, in independent experiments by a separate group [14]. Quasilaminarity of proton emission has been predicted in computational work [6] as a consequence of the shape of the Debye sheath accelerating the electrons at the back of the target. Particle-in-cell simulations [5,6] show that, in the presence of a spatially varying transverse electron distribution, the ion front in the accelerating Debye sheath becomes curved during the acceleration phase. This determines a 3D accelerating field with a strong radial component, which becomes progressively more important away from the axis, ultimately leading to quasilaminar flow [6].

The experimental results show that the emitting area is considerably larger than the laser focal spot size. In thin targets, electrons can acquire transverse momentum and spread transversely across the target, leading to an extended Debye sheath, due to the "fountain effect" driven by magnetic fields near the back surface [5]. In addition to this effect, while refluxing through the target [3], electrons can acquire transverse momentum due to reflections from curved sheaths. In thick targets, intrinsic divergence of the electron beam produced at the front of the

target can also be responsible for the large emission region observed. As a matter of fact, the 20°–30° electron beam divergence reported in various experiments [15] is broadly consistent with the emission area inferred at RAL.

In conclusion, experiments investigating multi-MeV proton emission from thin foils irradiated with ultra-intense laser pulses have provided new insight on the characteristics of the proton source. The protons in the energy range considered are emitted from an extended area of radius ~ 100 μm, in a quasilaminar fashion, with very low emittance. For projection purposes, the emission properties are equivalent to those of a much smaller virtual source located several hundred microns in front of the target. This has been proven by careful magnification checks employing proton backlighting of periodic, cold structures. This evidence is reinforced by measurements of proton emission employing targets preheated by moderate-intensity irradiation, also confirming emission from a similar-sized area. The finding is of great importance for applications employing the protons as a high resolution backlighting or heating source.

[1] E. L. Clark *et al.*, Phys. Rev. Lett. **84**, 670 (2000); A. Maksimchuk *et al.*, Phys. Rev. Lett. **84**, 4108 (2000); R. D. Snavely *et al.*, Phys. Rev. Lett. **85**, 2945 (2000); M. Zepf *et al.*, Phys. Rev. Lett. **90**, 064801 (2003).

[2] A. J. Mackinnon *et al.*, Phys. Rev. Lett. **86**, 1769 (2001).

[3] A. J. Mackinnon *et al.*, Phys. Rev. Lett. **88**, 215006 (2002).

[4] S. Hatchett *et al.*, Phys. Plasmas **7**, 2076 (2000); H. Ruhl *et al.*, Plasma Phys. Rep. **27**, 363 (2001); T. Zh. Esirkepov *et al.*, Phys. Rev. Lett. **89**, 175003 (2002).

[5] A. Pukhov, Phys. Rev. Lett. **86**, 3562 (2001).

[6] S. Wilks *et al.*, Phys. Plasmas **8**, 542 (2001).

[7] M. Roth *et al.*, Phys. Rev. Lett. **86**, 436 (2001).

[8] M. Borghesi *et al.*, Phys. Plasmas **9**, 2214 (2002); M. Borghesi *et al.*, Phys. Rev. Lett. **88**, 135002 (2002).

[9] J. A. Cobble *et al.*, J. Appl. Phys. **92**, 1775 (2002).

[10] S. J. Gitomer *et al.*, Phys. Fluids **29**, 2679 (1986).

[11] D. West and A. C. Sherwood, Nature (London) **239**, 157 (1972).

[12] J. F. P. Ziegler, J. P. Biersack, and U. Littmark, *The Stopping and Range of Ions in Solids* (Pergamon, New York, 1996).

[13] S. Humpries, Jr., *Charged Particle Beams* (Wiley and Sons, New York, 1990).

[14] M. Roth *et al.*, Plasma Phys. Controlled Fusion **44**, B99 (2002).

[15] K. B. Wharton *et al.*, Phys. Rev. Lett. **81**, 822 (1998); J. Santos *et al.*, Phys. Rev. Lett. **89**, 025001 (2002).